Electromagnetic Science
vol. 1, no. 1, 0010091, March 2023
https://doi.org/10.23919/emsci.2022.0009

Review

Transmitarray and Reflectarray Antennas Based on a Magnetoelectric Dipole Antenna

Kwai-Man Luk[1,2] and Bingjie Xiang[1,2]

1. *City University of Hong Kong, Hong Kong SAR, 999077, China*
2. *City University of Hong Kong Shenzhen Research Institute, Shenzhen 518057, China*

Corresponding author: Kwai-Man Luk, Email: eekmluk@cityu.edu.hk.
Received October 31, 2022; Accepted February 20, 2023; Published Online March 31, 2023.

Abstract — This paper presents a review of transmitarray (TA) and reflectarray (RA) antennas based on the magnetoelectric (ME) dipole antenna structure. First, the basic operating principles of ME dipole, TA and RA antennas are introduced. Next, ME-dipole-based TA and RA designs are discussed, with four antenna designs presented in detail, including two fixed-beam TA designs with high aperture efficiencies and two reconfigurable designs with a beam-scanning capability. The techniques involved in these designs are also analyzed to provide insight into the ME-dipole-based TA and RA designs. The simulated and measured results of the reported prototypes show that the introduction of the ME dipole antenna significantly broadens the bandwidths of the TA and RA antennas not only in the fixed-beam designs but also in the reconfigurable designs. The ME-dipole-based TA and RA designs reported in this paper are compared to highlight their benefits and limitations. Future possible research directions and challenges are also discussed.
Keywords — Beam scanning, High aperture efficiency, ME dipole, RA, TA, Wideband.
Citation — Kwai-Man Luk and Bingjie Xiang, "Transmitarray and Reflectarray Antennas Based on a Magnetoelectric Dipole Antenna," *Electromagnetic Science*, vol. 1, no. 1, article no. 0010091, 2023. doi: 10.23919/emsci.2022.0009.

I. Introduction

With the great success of mobile communications and the prosperity of the internet of things (IoT), the spectrum below 6 GHz has become very crowded and congested [1]–[3], which motivates the use of higher frequency bands in wireless communications. In addition, a higher operating frequency usually means a wider absolute bandwidth, lower latency and a higher data rate, which are also desired in the beyond fifth generation (B5G) and sixth generation (6G) wireless communication systems [4]–[6]. Moreover, imaging and remote sensing systems based on higher operating frequencies have also attracted much attention in academic and engineering fields [7], [8]. However, the free-space path loss of an electromagnetic wave expressed as the ratio of the received power to the transmitted power on a linear scale is given by [9]:

$$\frac{P_r}{P_t} = \frac{G_t G_r \lambda^2}{(4\pi D)^2} \tag{1}$$

where G_t and G_r are the transmitter and receiver antenna gains, λ is the signal wavelength, and D is the distance between the transmitter and the receiver. The path loss will gradually increase with increasing operating frequency. Hence, high-gain antennas are appreciated in high-frequency wireless applications because they can compensate for the high path loss. However, the coverage is limited if a high-gain antenna is applied, which impedes its applications. Therefore, high-gain antennas with a beam-scanning capability are promising solutions [10]–[12] to this problem because they can simultaneously compensate for the high path loss and obtain broad coverage.

Introducing the phased array technique is the most straightforward method to enhance the antenna gain [12]. However, complex and lossy feeding networks are involved to provide excitation for each element with the desired phase and magnitude [13], [14]. Even though some digital phased array systems show good performance, the expensive RF front end severely limits their applications [15]. Taking advantage of the spatial feeding method, transmitarray (TA) and reflectarray (RA) antennas have the characteristics of a planar structure, easy fabrication, low cost and large scanning angles [16], [17]. Since the element of the TA or RA is excited by the illumination from a primary source, the feeding networks in a phased array can be avoided, which makes these arrays suitable for high-frequency and large-aperture antennas. The major disadvantage of TA and RA antennas is their narrow bandwidth, which is limited by the differential spatial phase delay and the bandwidth of the element [18], [19]. The main issue re-

garding the former characteristic is that the phase distribution of the aperture is usually obtained according to the center frequency, and the best phase distribution is frequency-dependent. When the frequency deviates from the center frequency, a phase error occurs, leading to performance deterioration. To solve this problem, the true-time-delay line structure and multifrequency compensation strategy have been introduced [20]. The main issue regarding the latter characteristic is that the elements are usually based on a patch antenna and a frequency-selective surface (FSS) structure [21]–[23]. These introduced elements are intrinsically narrowband, which leads to the limited bandwidth of TA and RA antennas. Even though multiresonance elements and multilayer structures [24]–[26] have been used to broaden the bandwidth of an FSS, the complex structures make the assembly difficult, especially for higher frequency bands because air gaps are usually required. Moreover, wideband FSS-based TA and RA antennas with reconfigurability and a beam-scanning capability are difficult to design.

Inspired by the complementary antenna concept, the magnetoelectric (ME) dipole antenna was proposed to develop a novel wideband antenna for mobile communications [27]. The advantages of ME dipole antennas are a wide operating bandwidth, identical radiation patterns in the E- and H-planes, a simple structure and low cross-polarization levels. The typical operating bandwidth of an ME dipole antenna is more than 50%, within which the radiation patterns and antenna gain are stable. These advantages make the ME dipole antenna very popular, and it has been enhanced to exhibit dual linear polarization [28], circular polarization [29], dual-band operation [30], filtering integration [31], etc. Moreover, the ME dipole antenna also shows good performance in high-frequency bands, even up to the millimeter-wave and terahertz bands [32]–[36].

Recently, ME dipole antennas have been applied as elements in TA and RA designs to replace patch antennas and FSS structures. Compared to the conventional designs, the operating bandwidths of the proposed ME-dipole-based designs have been significantly improved. In addition, within the operating bandwidth, other performance parameters, including the aperture efficiencies, cross-polarization levels, sidelobe levels and beam-scanning capability, are very stable and comparable to or even better than those of the conventional designs.

This paper is organized as follows. Section II presents the basic operating principles of the ME dipole, TA and RA antennas. Then, the fixed-beam TA and RA designs based on an ME dipole antenna are introduced, focusing on a TA antenna with a 2-bit resolution and a TA antenna with circular polarization. Next, the beam-scanning designs are shared in Section III, focusing on a low-cost reconfigurable RA (RRA) and a low-profile reconfigurable TA (RTA). Subsequently, all the reported prototypes based on ME dipole antennas are compared in Section IV to highlight their merits and limitations. Possible future research directions and challenges are also discussed. In Section V, a brief conclusion is given.

II. Operating Principles

1. ME dipole antenna

The basic structure of the ME dipole antenna was first developed in [27] based on the complementary antenna concept. This structure is illustrated in Figure 1, which consists of two horizontal patches with inner edges connected to the ground, a Γ-shaped probe and a ground plane. The two planar horizontal patches, working as an x-polarized electric dipole, are placed at a height of a quarter wavelength above the ground plane. The two vertical shorted walls and the ground plane work together as a y-polarized magnetic dipole. Finally, the Γ-shaped probe is used to excite the two resonances and provide impedance matching. By properly arranging the two resonances, the operating bandwidth can be easily enhanced to approximately 44% [27].

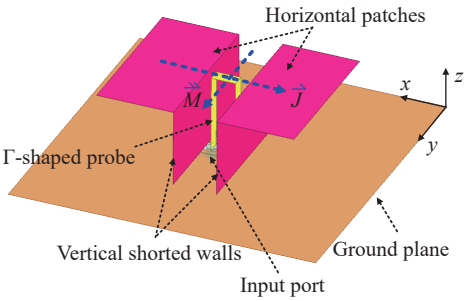

Figure 1 Structure of the ME dipole antenna [27].

In addition, the electric dipole and the magnetic dipole are orthogonal to each other and simultaneously excited, forming a complementary antenna structure. Therefore, identical radiation patterns and low cross-polarization levels can be realized in both principal planes, enabling the antenna to be very suitable for base station applications [37]. Note that the aperture-coupling method is widely used to excite ME dipole antennas due to its simple structure, ease of fabrication and compatibility with transmission line structures for higher frequency bands, such as substrate-integrated waveguides (SIWs) [32], substrate-integrated coaxial lines (SICLs) [38] and groove gap waveguides (GGWs) [39].

2. TA and RA antennas

The basic structures of the TA and RA antennas are shown in Figure 2. Different from the phased array, a primary source is placed at the focal point, and the elements of the TA and RA antennas are excited by the illumination from the primary source.

For a TA antenna, the electromagnetic wave from the primary source will be transmitted by the TA element with a deliberately designed phase delay. The goal is to transform the spherical wave from the primary source into a plane wave at the radiating aperture of the TA. Therefore, each element needs to provide an independent phase shift,

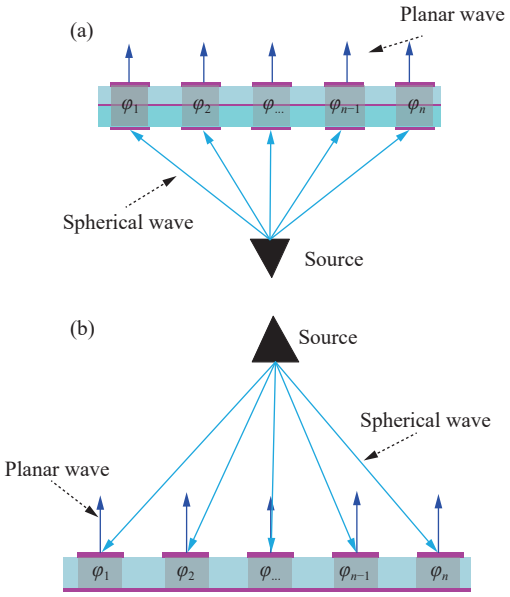

Figure 2 Illustration of the operating principles of (a) the TA antenna and (b) RA antenna.

which can be calculated by [19]:

$$\varphi_{ij} = k(R_{ij} - \vec{r}_{ij} \cdot \hat{r}_o) + \varphi_0 \tag{2}$$

where i and j are the column and row indexes of the (i, j)th element. φ_{ij} is the transmission phase for the (i, j)th element, and R_{ij} is the distance between the phase center of the primary source and the (i, j)th element. $\hat{r}_o$ is the unit vector of the main beam direction, and $\vec{r}_{ij}$ is the position vector of the (i, j)th element in the TA coordinates. φ_0 is a constant phase, indicating that a relative transmission phase is required.

Different from the TA antenna design, in the RA antenna design, the electromagnetic wave from the primary source will be reflected by the RA element with a deliberately designed phase delay [18]. The desired phase shift of the RA element can also be calculated by (2). Note that the offset feed method is usually used in RA designs to reduce feed blockage.

With reference to (2), when the position of the primary source and the beam direction are determined, the phase shift of an element can be obtained, which means that the phase distribution on the TA or RA aperture is determined. Additionally, perfect compensation of the phase delay from the primary source by the element is desired, which requires the element to provide a phase shift range of over 360°. This is difficult because good magnitude responses should be maintained for all phase states. However, there are infinite phase states in the continuous phase compensation scheme. To solve this problem, a discrete phase compensation strategy is proposed. The discrete phase strategy means that the element can only provide several discrete phase states. It has recently been drawing great interest due to its simple structures and great potential in reconfigurable designs. In discrete designs, the constant phase φ_0 should be optimized to alleviate the performance deterioration introduced by the finite phase states.

Moreover, based on (2), different compensation phase shifts should be assigned for each element when the main beam direction is differently designed in beam-scanning applications. Therefore, beam-scanning applications require dynamic adjustment of the phase responses of the elements, regardless of whether they are electrical components, liquid crystals or microelectromechanical systems (MEMS) [40]–[42].

To evaluate the radiation performance of a TA or RA antenna, the array-theory method is employed. The far-field radiation can be obtained by:

$$E(\theta,\varphi) = \sum_{i=1}^{M}\sum_{j=1}^{N} \cos^{q_e}\theta \frac{\cos^{q_f}\theta_{f(i,j)}}{R_{ij}} \times e^{-jk\left(R_{ij}-\vec{r}_{ij}\cdot\hat{r}_o\right)} \cos^{q_e}\theta_e(i,j)\, e^{j\varphi_{ij}} \tag{3}$$

The radiation patterns of the element and primary source are modeled as $\cos^{q_e}\theta_{e(i,j)}$ and $\cos^{q_f}\theta_{f(i,j)}$, respectively. φ_{ij} represents the phase delay introduced by the (i, j)th element. Furthermore, the directivity of the antenna can be calculated by

$$D = \frac{4\pi |E(\theta_m,\varphi_m)|^2}{\int_0^{2\pi}\int_0^{\pi} |E(\theta,\varphi)|^2 \sin\theta \, \mathrm{d}\theta \mathrm{d}\varphi} \tag{4}$$

where (θ_m, φ_m) is the main beam direction.

III. ME Dipole Antenna in TA and RA Designs with Fixed Beams

In this section, the ME-dipole-based TA and RA designs with fixed beams will be discussed. According to the phase compensation technique, this section is divided into two parts: linearly polarized (LP) and circularly polarized (CP) designs.

1. Wideband LP TA designs

1) Wideband TA antenna

The first ME dipole in a TA design was implemented in 2018 by Z. W. Miao *et al.* [43]. The proposed element structure is composed of two aperture-coupled ME dipole antennas (one for receiving, the other for transmitting) with an inserted folded SIW delay line. A phase shift range of over 360° can be achieved by varying the length of the delay line to provide a continuous phase compensation scheme. The prototype was fabricated by low-temperature co-fired ceramic (LTCC) technology due to its complex structure. The proposed prototype can obtain a 3-dB gain bandwidth of 24% and a peak aperture efficiency of 50%.

2) Wideband 1-bit TA antenna

To achieve a simple structure, two ME dipole antennas fed by L-shaped probes are connected by a feeding pin [44], as shown in Figure 3. To provide the phase shift, the feeding strip of the transmitting ME dipole antenna is rotated by 180° to achieve a 1-bit resolution. The authors also claimed that

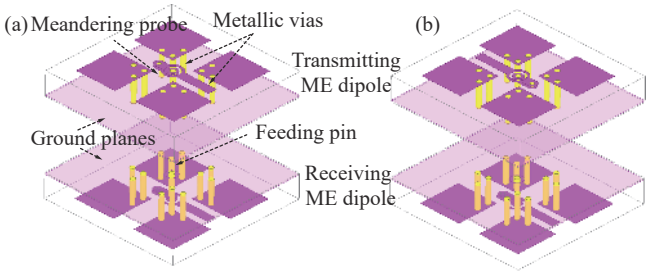

Figure 3 Structures of the TA element [44]. (a) State 1; (b) State 2.

the cross-polarization levels can be suppressed when the transmitting and receiving layer feeding strips are simultaneously manipulated. The prototype was fabricated by using standard printed circuit board (PCB) technology. Even though the prototype has a wide operating bandwidth of 47%, its measured peak aperture efficiency is only 28% due to the 1-bit compensation scheme. Based on this simple structure, many variants have been implemented, such as dual LP TA antennas [45], CP TA antennas [46], and multibit TA antennas [47].

3) Wideband 2-bit TA antenna

As mentioned in Section II, even though an over 360° phase shift range is desired for the element, two major challenges are encountered in TA and RA designs. The first is linearity of the phase response, which is difficult to achieve within a wide operating bandwidth. The second is the magnitude response. A large phase shift range usually introduces higher insertion loss in some phase states, limiting the TA and RA performance. Therefore, even though discrete phase compensation schemes suffer from performance deterioration, they are widely applied in TA or RA designs due to their simple structure and fewer requirements for the element. In addition, since the element can only support several discrete working states, the phase and magnitude responses of all working states can be optimized to guarantee better performance.

According to the analysis in [48], [49], the 1-bit resolution compensation scheme, which means that the element can only provide two ($2^1 = 2$) states, suffers an approximately 3-dB gain loss compared with the continuous compensation scheme. In contrast, the 2-bit and 3-bit resolutions need to provide four ($2^2 = 4$) and eight ($2^3 = 8$) phase states, accompanied by 0.8 dB and 0.3 dB gain losses, respectively. Therefore, four additional phase states are needed for the 3-bit resolution to obtain a 0.5 dB gain enhancement compared to the 2-bit resolution, which is not economical. Moreover, the 2-bit digital-coding element is very suitable for reconfigurable intelligent surface (RIS) implementation considering the balance between system cost, design complexity and overall performance [16]. Therefore, TA and RA antennas with a 2-bit resolution are promising candidates for upcoming B5G and 6G wireless communication systems.

In [50], a 2-bit TA is proposed based on the ME dipole to simultaneously achieve high gain, high aperture efficiency and wide bandwidth. Its structure is shown in Figure 4. In this prototype, a wideband 90° phase shifter is proposed and inserted into two L-shaped probe-fed ME dipole antennas. Similar to [44], a 180° phase shift is obtained by rotating the feeding strip in the transmitting layer. Moreover, an additional 90° phase shift is achieved by inserting the reference line or the main line. Therefore, combining these two techniques, a progressive 90° phase shift can be obtained, demonstrating the 2-bit resolution capability. Note that three identical open stubs are applied here to change the phase slope. Therefore, four parallel phase responses can be achieved, as shown in Figure 5. In addition to the stable phase responses, the transmission losses of the four states are less than 1 dB within the whole operating bandwidth.

Since the proposed element can only provide four phase states, the strategy for assigning the phase of each element is given below:

$$\begin{cases} \varphi \le 45^\circ \text{ or } \varphi > 315^\circ \rightarrow \varphi = 0^\circ \\ 45^\circ < \varphi \le 135^\circ \rightarrow \varphi = 90^\circ \\ 135^\circ < \varphi \le 225^\circ \rightarrow \varphi = 180^\circ \\ 225^\circ < \varphi \le 315^\circ \rightarrow \varphi = 270^\circ \end{cases} \tag{5}$$

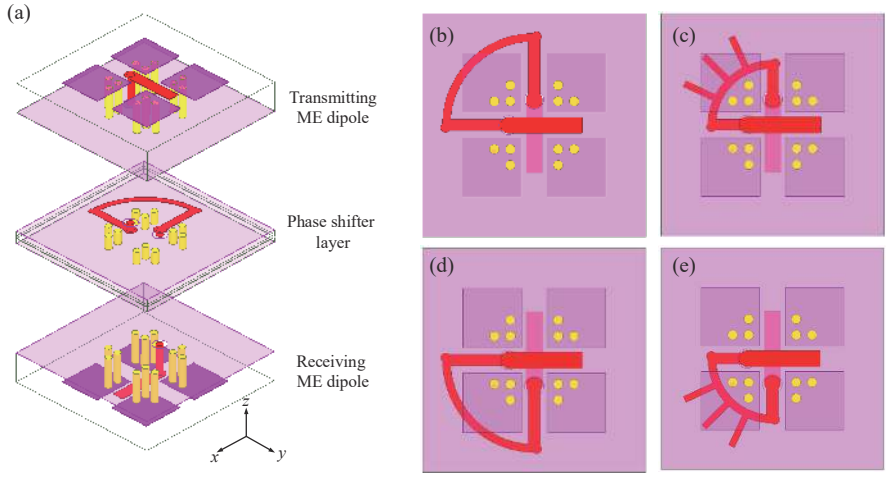

Figure 4 (a) Configuration of the TA element [50]; (b) State 1 (0°); (c) State 2 (90°); (d) State 3 (180°); (e) State 4 (270°).

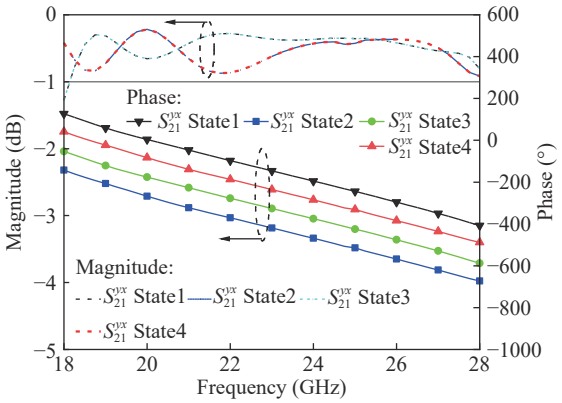

Figure 5 Simulated results of the elements [50].

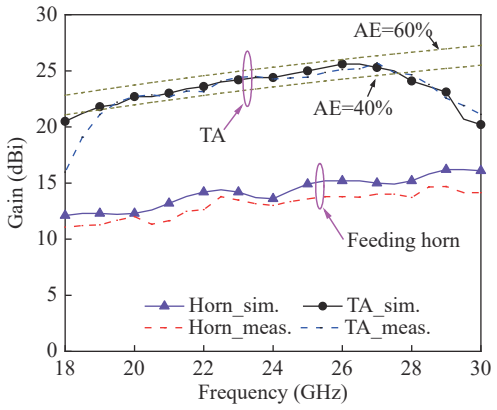

Figure 6 Measured results of the prototype in [50].

In this TA design, the constant phase φ_0 is optimized by the multifrequency compensation strategy to achieve minimum weighted phase errors. The cost function of the optimizing algorithm is shown below:

$$\mathrm{CF} = \sum_{f_i=1}^{Q} \sum_{i=1}^{M} \sum_{j=1}^{N} \frac{\dfrac{\cos^{q_{f/2}}\theta_{f(i,j)}}{R_{ij}}}{\max\left(\dfrac{\cos^{q_{f/2}}\theta_{f(i,j)}}{R_{ij}}\right)} \cdot \varphi_{\mathrm{error}}(i,j,f_i) \quad (6)$$

where $\varphi_{\mathrm{error}}(i,j,f_i)$ is the phase error of the (i,j)th element at frequency point f_i. Q represents the number of sampled frequency points ($Q = 3$ in this case).

The simulated and measured results of the prototype are shown in Figure 6. The fabricated prototype is composed of 144 elements, which can obtain a peak gain of 25 dBi. An approximately 11 dB gain enhancement can be observed when the designed 2-bit TA antenna is employed. The measured aperture efficiency is approximately 53%, which is approximately twice that in [44]. The achieved aperture efficiencies are even comparable to those obtained with the 3-bit or continuous phase compensation scheme [43], [51]. The obtained 3-dB gain bandwidth is approximately 38%. The radiation patterns of the prototype at 24 GHz are shown in Figure 7. The prototype can achieve low sidelobe levels and low cross-polarization levels in both principal planes.

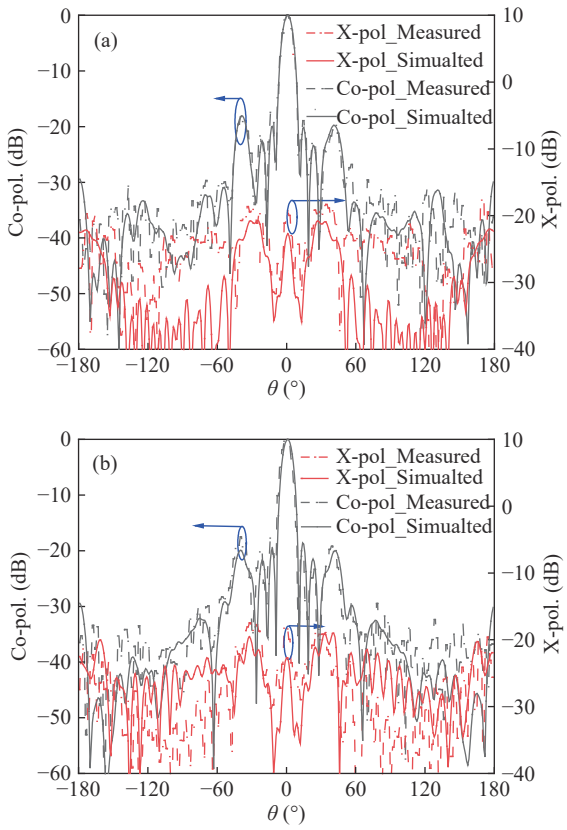

Figure 7 Radiation patterns at 24 GHz [50]. (a) E-plane; (b) H-plane.

2. Wideband CP RA and TA antennas

The geometric phase is widely used in CP TA and RA designs to compensate for the phase delay. According to the analysis in [52], [53], when a CP wave illuminates a CP element, the phase shift of the transmitted wave or the reflected wave can be flexibly controlled by rotating the elements.

1) Wideband CP RA antenna

Based on the basic CP ME dipole antenna in [32], a simple CP RA element is proposed by connecting the two diagonal patches with a narrow strip, as shown in Figure 8 [54]. This narrow strip can introduce a 180° reflected phase difference for two orthogonal LP waves to obtain the geometric phase. By rotating the element from 0° to 180°, a 360° phase shift range is obtained for the reflected phase. Hence, a continuous phase compensation strategy can be applied to generate a pencil beam with circular polarization. The achieved peak aperture efficiency is 60%, and the axial ratio (AR) bandwidth is 42%.

2) Wideband CP TA antenna

Additionally, based on the geometric phase, a wideband CP TA antenna is proposed in [55], where LP and left-hand circularly polarized (LHCP) ME dipole antennas are used as the receiving and transmitting parts, respectively. The structure of the proposed element is shown in Figure 9. The techniques of corner-truncation and hook-shaped strips are

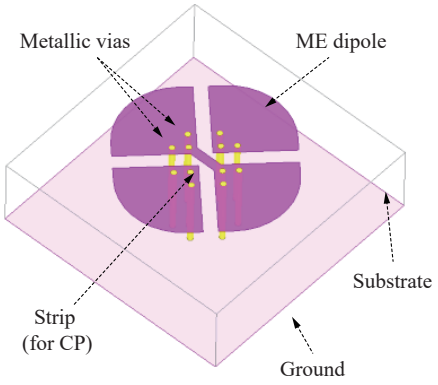

Figure 8 Structure of the CP RA element [54].

employed to generate CP radiation in the transmitting antenna. Different from the conventional feeding method, inductive and capacitive couplings are combined to provide differential currents and simultaneously feed the magnetic and electric dipoles. This special feeding method allows the feeding pin to be located at the center of the element. Therefore, the CP ME dipole antenna of the transmitting layer can be freely rotated to obtain the geometric phase while the receiving antenna remains unchanged. The phase and magnitude responses of the elements are shown in Figure 10. Low insertion, a stable phase shift and an over 360° phase shift range can be achieved within the wide operating bandwidth. Therefore, a continuous phase compensation strategy can be applied to the TA aperture to achieve a CP pencil beam.

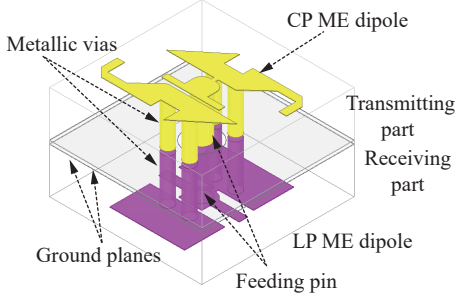

Figure 9 Structure of the CP TA element [55].

In addition, this proposed element can convert spherical LP waves into planar LHCP waves, which alleviates the design burden on the feeding source since only an LP source is needed. Therefore, a fully metallic 2 × 2 LP ME dipole array is proposed to illuminate the TA. The measured results of the CP TA are shown in Figure 11. The prototype can achieve a peak gain of 25.6 dBic with a peak aperture efficiency of 44%. The obtained 1-dB and 3-dB gain bandwidths are approximately 15% and 33%, respectively. The AR value within the operating bandwidth is less than 2 dB, demonstrating good LHCP radiation. The radiation patterns at the center frequency (32 GHz) are shown in Figure 12. Stable pencil beams with low cross-polarization and sidelobe levels are achieved in both principal planes.

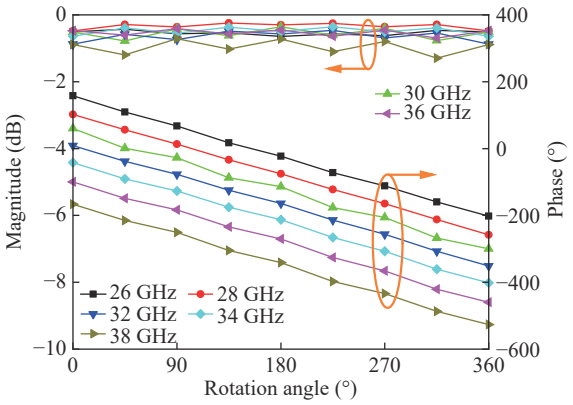

Figure 10 Simulated results of the CP TA element [55].

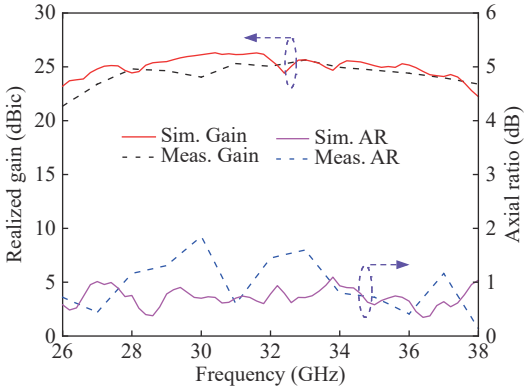

Figure 11 Measured results of the wideband CP TA antenna [55].

IV. ME Dipole Antenna in TA and RA Designs with Scanning Beams

As mentioned in Section I, RTA and RRA antennas with a beam-scanning capability are more practical in wireless communications, imaging, sensing, and medical monitoring applications. According to the realization of the beam-scanning property, this section is divided into two parts: designs enabled by offset feed and those enabled by PIN diodes.

1. Beam scanning enabled by offset feed

The first method to achieve a beam-scanning capability is to place a set of source antennas near the focal point [56], as shown in Figure 13. The offset feeding sources will cause the main beam direction of the TA or RA antenna to deviate from the broadside direction with a tilt angle of θ. The tilted beam direction can be roughly calculated by the following equation [57]:

$$\theta = d/f \tag{7}$$

where f is the focal length of the TA antenna and d is the distance between the source antenna and the focal point. However, the offset feeding source inevitably brings phase errors, which limits the beam-scanning performance, including the scanning angles, scan loss and sidelobe level.

In [58], a novel rotationally symmetric TA element is

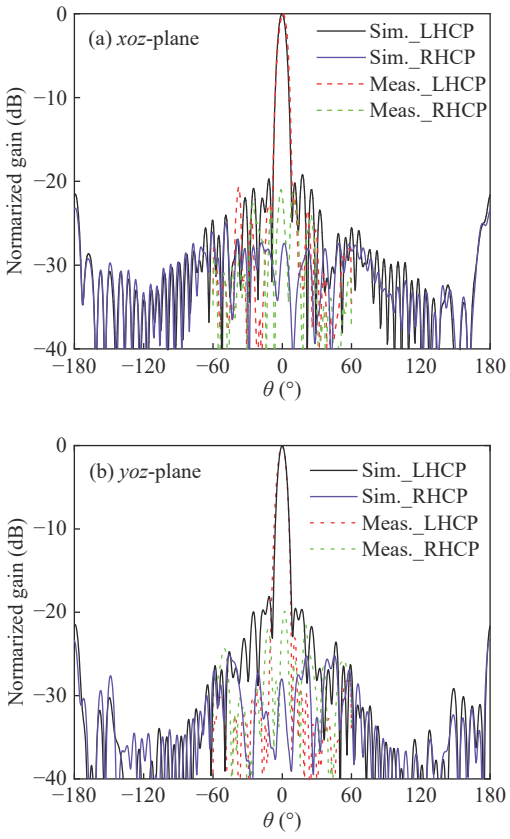

Figure 12 Measured results of the wideband CP TA antenna [55]. (a) *xoz*-plane; (b) *yoz*-plane.

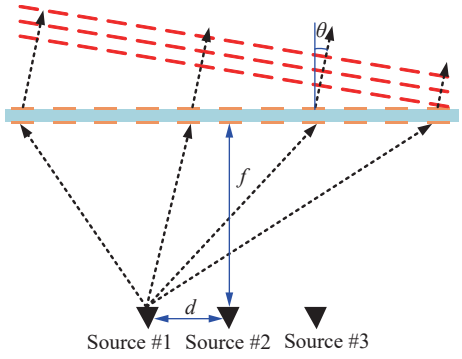

Figure 13 Illustration of beam scanning by offset feed.

proposed by combining two aperture-coupled ME dipole antennas with a cavity transition. Similar to [32], a narrow strip is employed to connect the diagonal patches to provide CP radiation to the transmitting ME dipole, and an LP ME dipole antenna is used as the receiving part. The cavity transition, composed of two cavities and an inserted metallic via, is used to realize good impedance matching between the transmitting and receiving ME dipole antennas. This special transition also enables the transmitting element to rotate freely to obtain the geometric phase while the receiving element can remain unchanged. Different from [55], seven collinear LP ME dipole antennas are used as the primary source to illuminate the TA aperture to obtain a one-dimensional (1-D) CP beam-scanning performance. In addition, the bifocal strategy is adopted to reduce the gain drop at large scanning angles. Finally, the prototype can obtain a 3-dB gain bandwidth of 33% with an aperture efficiency of 24%. Seven CP directive pencil beams are generated, pointed toward −29°, −19°, −9°, 0°, 9°, 19°, and 29° at 27 GHz, providing a 3-dB beam coverage of ±33°.

2. Beam scanning enabled by a PIN diode

The second method to achieve reconfigurable designs is to integrate PIN diodes into the TA or RA element to dynamically control its phase response. Compared to the former method, this method can implement two-dimensional (2-D) beam scanning with higher resolution and more flexibility.

1) Wideband CP RRA with a 1-bit resolution

Inspired by [54], four PIN diodes are etched on the cross strip of the CP ME dipole to propose a wideband RRA element [59], as shown in Figure 14. A metallic shorting via is placed at the center of the cross strip to provide the DC voltages. The RF and DC ground planes are directly connected, leading to the DC voltage of the four patches being 0 V. Two diagonal PIN diodes are arranged reversely as a pair, and the two orthogonal pairs of PIN diodes are also arranged reversely. Therefore, by applying a positive or negative DC voltage to the center metallic via, one pair of PIN diodes is switched ON while the other is switched OFF, forming the CP ME dipole proposed in [54]. By selecting which pair is to be switched ON, the element is equivalently rotated by 90°, introducing a 180° phase shift into the reflected phase. Therefore, the proposed element can provide a 1-bit resolution for the CP wave. The fabricated prototype can achieve a peak aperture efficiency of 24% with an AR bandwidth of 32%. Moreover, the RRA can obtain a 2-D scanning capability with scanning angles up to 60° and a scan loss of less than 3.1 dB.

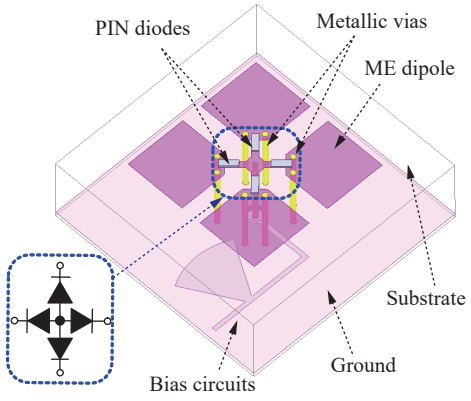

Figure 14 Structure of the 1-bit CP RRA element [59].

2) Wideband low-cost RRA with a 1-bit resolution

TA and RA antenna designs are usually composed of hundreds or even thousands of elements. When many PIN diodes are involved in each element, the cost of the system will dramatically increase, which severely limits its application. Therefore, how to reduce the number of PIN diodes is an urgent problem and worthy of research.

To reduce the number of PIN diodes, a low-cost RRA is proposed in [60] by using a single PIN diode in each ME-dipole-based element. The structure of the element is illustrated in Figure 15. Two metallic strips are applied to arrange the electrically controlled PIN diode, denoted Strip I and Strip II. Strip I connects the left two patches, which are shorted to the ground plane with a 0 V DC voltage. A metallic via, isolated from the ground, is loaded at Strip II to provide DC voltages. The PIN diode is soldered between Strip I and Strip II to realize reconfigurability. The DC bias circuits are composed of narrow metallic strips, which are loaded by fan-shaped open stubs to reduce the effects of the bias circuits within a wide bandwidth. Since Strip I is the DC ground, the working states of the PIN diode can be controlled by the voltages provided by the bias circuits. When Strip II is biased with a negative voltage (−3.3 V), the PIN diode is switched ON, and the left endpoint of Strip II is shorted. When Strip II is biased by a positive voltage (+ 3.3 V), the PIN diode is switched OFF, and the left endpoint of Strip II is open. Therefore, a 180° phase difference can be obtained within a wide bandwidth by employing different bias voltages. The simulated results of the element are shown in Figure 16, which illustrates that the two working states have a stable phase difference of 180° with a maximum ripple of 20°.

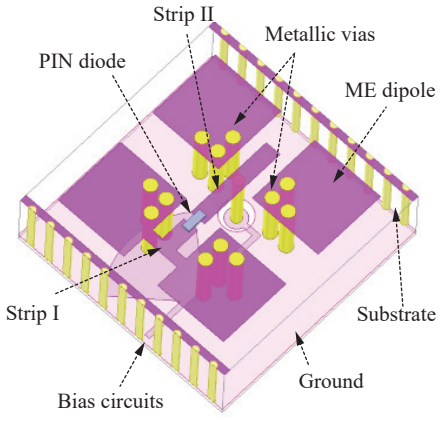

Figure 15 Structure of the 1-bit RRA element [60].

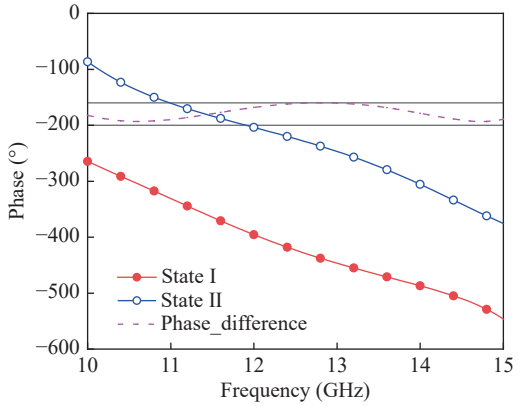

Figure 16 Simulated phase response of the proposed RRA element [60].

A photograph of the prototype is shown in Figure 17, and its measured results are shown in Figure 18. According to this figure, the antenna gain of the RRA increases with frequency, accompanied by a peak gain of 20 dBi and a peak aperture efficiency of 24%. The obtained 3-dB gain bandwidth is approximately 38%, which is much wider than that of the conventional RRA designs. Moreover, different phase compensation schemes are applied at different frequency points to explore the potential of the proposed RRA. This technique can alleviate the differential spatial phase delay in wideband RRA and RTA designs. The scanning performance is shown in Figure 19, demonstrating a scanning capability of ±60° in the E-plane and 0–60° in the H-plane. The maximum scan losses are 4.5 dB and 5.5 dB in the E- and H-planes, respectively. The scanning performance in the H-plane is mainly limited by feed blockage.

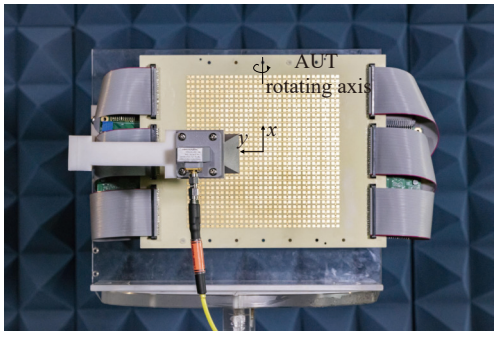

Figure 17 Photograph of the proposed RRA [60].

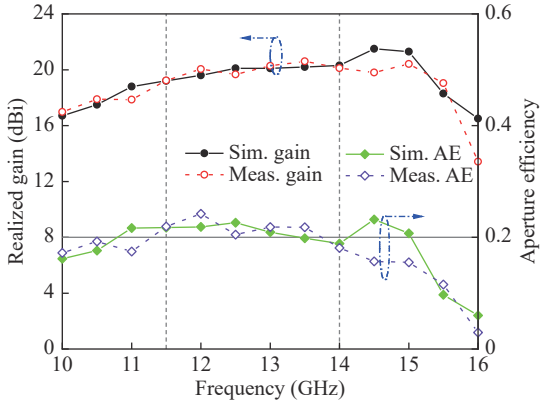

Figure 18 The Simulated and measured antenna gain of the proposed RRA [60].

3) Wideband low-profile RRA with a 1-bit resolution

The design of an RA antenna is usually easier than that of a TA antenna because the reflected magnitudes are generally equal to 1, and only the reflected phase shift should be deliberately designed. However, an RA antenna will suffer blockage of the feeding source, which will introduce blind regions. To solve this problem, an RTA antenna based on the ME dipole antenna element is proposed, whose structure is shown in Figure 20 [61]. A conventional L-shaped probe is employed to feed the transmitting part. In the receiving part, two PIN diodes are reversely deployed on the

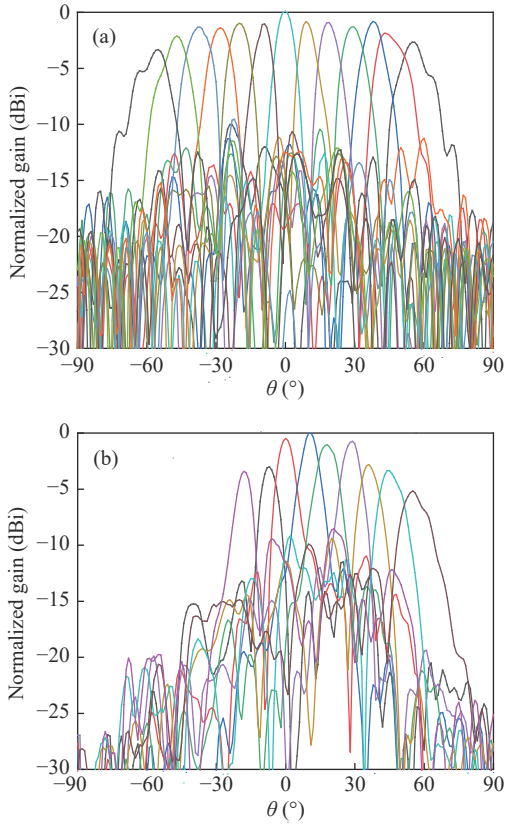

Figure 19 Measured radiation patterns at 12.5 GHz of the proposed RRA antenna [60]. (a) E-plane; (b) H-plane.

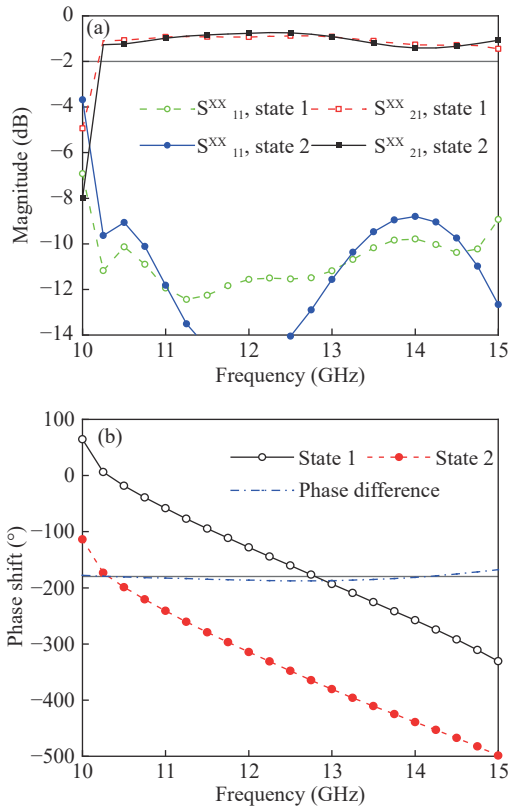

Figure 21 Simulated performance of the proposed RTA element [61]. (a) Amplitude; (b) Phase.

two sides of the central feeding pin. The feeding pin is connected to the bias circuits by a narrow copper line and a fan-shaped open stub, leading to connection in DC but isolation in RF. When the feeding pin is biased with a positive voltage (+3.3 V), the left PIN diode is switched ON while the right diode is switched OFF, and vice versa when the feeding pin is biased with a negative voltage (−3.3 V). Therefore, the direction of the excitation current can be reversed by different bias voltages, leading to a 180° phase difference (1 bit). The simulated results of the proposed element are shown Figure 21. Similar transmission performance can be observed for the two working states, except for a 180° difference in transmission phases.

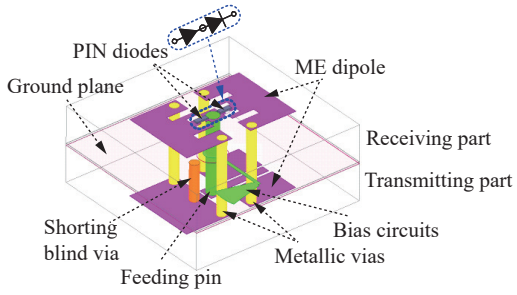

Figure 20 Structure of the proposed RTA element [61].

To reduce the profile of the TA antenna, the folded structure shown in Figure 22 has been introduced. The primary source radiates *y*-polarized waves that are totally reflected by the TA to the reflective polarization conversion surface (RPCS). Then, the RPCS reflects the waves again with polarization conversion. Therefore, the *y*-polarized waves are transformed into *x*-polarized waves and propagate to the TA aperture again. Then, the *x*-polarized waves are transmitted by the TA element with the deliberately designed phase delay to generate directive pencil beams. Because of the folded structure, the profile of the folded TA is reduced to one-third of the focal length.

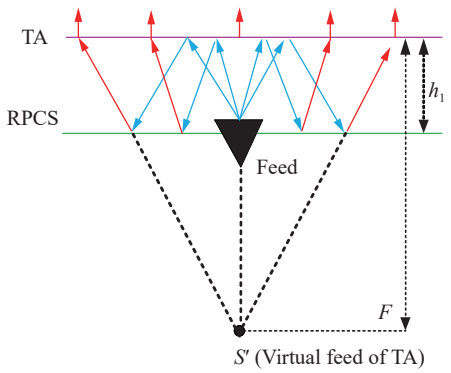

Figure 22 Structure of the proposed folded RTA antenna [61].

The structure of the RPCS element is shown in Figure 23, which consists of a C-shaped resonator, a metallic ground plane and a supporting substrate. This structure can convert the polarization of electromagnetic waves into the

orthogonal polarization within a wide bandwidth. A photograph of the prototype is shown in Figure 24. Benefitting from the folded structure, the profile of the antenna is reduced to approximately 38.5 mm, which is much lower than that of the conventional TA designs. A DC connector is used to provide the DC connection between the antenna board and the field programmable gate array (FPGA) digital board. A standard rectangular waveguide is used to feed the TA antenna.

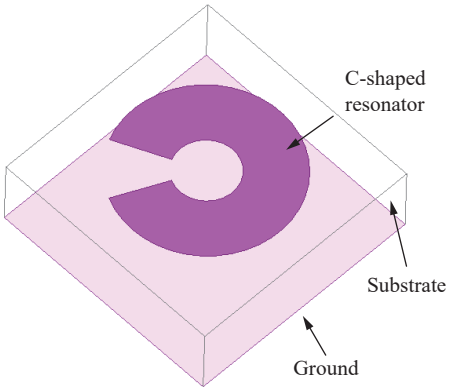

Figure 23 Structure of the proposed RPCS element [61].

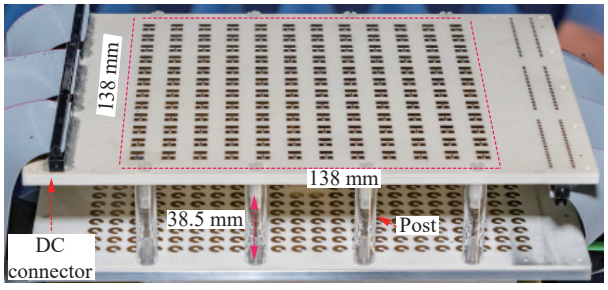

Figure 24 Photograph of the proposed low-profile RTA [61].

To alleviate the performance deterioration introduced by discrete phase states, the phase error needs to be minimized. The weighted phase error in this paper is calculated by [61]

$$W = \frac{1}{MN}\sum_{i=1}^{M}\sum_{j=1}^{N}\cos^{q_e}(\theta_e)F_{ij}\varphi_{\text{error}}(i,j) \qquad (8)$$

where $\varphi_{\text{error}}(i,j)$ is the phase error of the (i,j)th element. F_{ij} is the amplitude of each TA element, which is obtained by full-wave simulation.

The simulated and measured results are shown in Figure 25. The proposed prototype achieves a peak gain of 19 dBi and an aperture efficiency of 20%. The measured 3-dB gain bandwidth is 37%. The scanning performance is shown in Figure 26. The prototype can scan from 0° to 40° in both the E- and H-planes. The scan loss is less than 2.7 dB, and the sidelobe levels are less than 6.2 dB. Note that the proposed prototype should have the capability of scanning from −40° to +40° in both principal planes because of the symmetry of the structure.

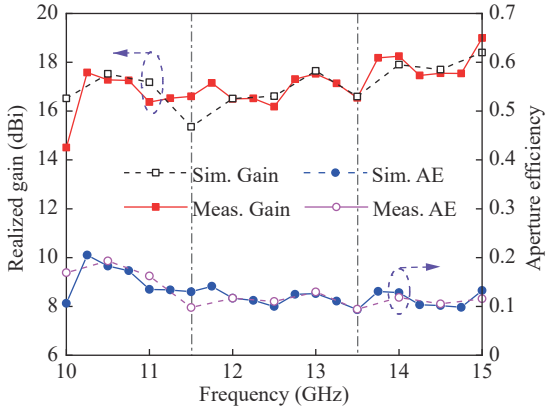

Figure 25 Simulated and measured results of the RTA antenna [61].

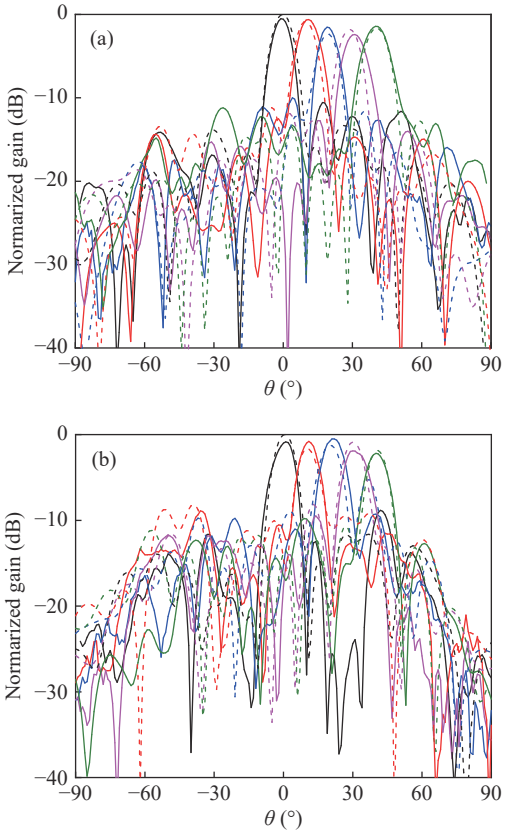

Figure 26 Simulated and measured radiation patterns at 12.5 GHz of the RTA antenna [61]. (a) E-plane; (b) H-plane.

V. Challenges and Future Research Work

The ME-dipole-antenna-based TA and RA antennas presented in this review are summarized in Table 1 to illustrate their advantages and limitations. According to this table, even though the ME dipole antenna has been successfully applied in TA and RA designs and their bandwidths are significantly enhanced, several key challenges remain for future research.

The first challenge is the high profile of TA antennas. The folded scheme has been successfully applied and reduces the profile to one-third of the focal length [61]. Addi-

Table 1 Summary table of the references for TA and RA antennas based on ME dipole antennas

Ref.	Frequency	TA/RA	Fabrication	H/D	Phase shift rangeof the element	Polarization	Peak aperture efficiency	3-dB gain bandwidth	Beam-steering
[43]	140G	TA	LTCC	1.866	>360	LP	50.12%	24.4%	No
[44]	27G	TA	PCB	1.07	1-bit	LP	28%	47%*	No
[45]	27G	TA	PCB	1.07	1-bit	Dual LP	31%	23%	No
[46]	27G	TA	PCB	1	Over 2-bit	CP	–	47%	No
[47]	27G	TA	PCB	1.07	Over 2-bit	LP	41%	33%	No
[50]	23G	TA	PCB	1	2-bit	LP	53%	38.7%	No
[54]	10G	RA	PCB	1.2	>360	CP	60%	42%	No
[55]	32G	TA	PCB	1.08	>360	CP	44%	34%	No
[58]	27G	TA	PCB	0.45	>360	CP	24.8%	33.3%	Yes (1-D)
[59]	10G	RA	PCB	1.05	1-bit	CP	24%	31.5%	Yes (2-D)
[60]	10G	RA	PCB	1.2	1-bit	LP	24%	38.4%	Yes (2-D)
[61]	10G	TA	PCB	0.28	1-bit	LP	20.5%	37.6%	Yes (2-D)

Note: *Defined by the 3-dB aperture efficiency.

tionally, the profile can be further reduced to one-fourth of the focal length when the feeding source is placed at the plane of the TA aperture [62]. However, this method introduces feed blockage in TA designs. Therefore, a new approach to reduce the profile of the TA and eliminate the blockage needs to be proposed. Inspired by the folded structure and virtual feed method, double phase compensation (DPCM) [63] can be introduced to further reduce the profile. This method may be combined with the ME dipole antenna to propose TA or RA designs with simultaneous ultralow profiles and wide bandwidths.

The second problem is the number of bits in the reconfigurable designs. To date, most wideband reconfigurable ME-dipole-based designs have been implemented with 1-bit resolution. Even though these designs can achieve beam-scanning performance in the whole operating bandwidth, they suffer deterioration in antenna performance, such as low aperture efficiencies, small scanning angles, large scan loss and high sidelobe levels. According to the analysis in Section II, 2-bit resolution is a good compromise between complexity and performance. Therefore, the designs with a 2-bit resolution would be promising for upcoming 6G wireless communication systems. At the same time, 2-bit resolution usually requires more PIN diodes, which will increase the systematic cost. Therefore, reducing the number of PIN diodes in 2-bit TA or RA antennas is worthy of research.

The third challenge is how to realize multiple functions within a single TA or RA design. Thus far, the proposed ME-dipole-based designs only focus on phase manipulation and realize a single function. Although some reconfigurable designs have been proposed, they only focus on the beam-scanning capability. A single RA or TA antenna with multiple functions, such as polarization conversion (linear polarization to orthogonal polarization, LP to CP), a beam-scanning capability and multibeam characteristics, would be a promising solution for future wireless communication systems. The dual-polarized design with an independently controllable 2-bit resolution is a potential solution to realize multifunctional characteristics [64]. Moreover, amplitude manipulation is also desirable in the TA and RA designs to achieve low sidelobe levels (SLLs), beam shaping and absorption in intelligent reflecting surface (IRS) applications. Therefore, these designs with multiple functions would be more attractive in practical applications.

The fourth challenge is the reconfigurability in the millimeter-wave and terahertz bands. To date, PIN diodes have been used to realize reconfigurability of ME-dipole-based TA and RA antennas. However, in the millimeter-wave and terahertz bands, the insertion loss of PIN diodes is severe, and the integration of reconfigurable components is difficult due to the small size of the antenna element. Complementary metal-oxide semiconductor (CMOS) technology would be a promising solution for RRA and RTA designs in the millimeter-wave and terahertz bands because the PIN diode and transistor can be fully integrated with CMOS technology.

The fifth challenge is the design complexity. At the microscopic level, ME-dipole-based TA or RA elements are more complex than other types of elements. This characteristic makes the element design more laborious and time-consuming. To solve this problem, machine learning methods can be used to estimate the electromagnetic response without full-wave simulation and combined with an optimization algorithm to speed up the design process. At the macroscopic level, machine learning methods can also be introduced to obtain the phase distributions for beam-shaping applications.

VI. Conclusions

This paper provides a thorough review of the TA and RA designs based on the ME dipole antenna structure. The introduction of the ME dipole antenna significantly broadens the operating bandwidths of the prototypes without sacrificing other antenna performance parameters. In addition, bandwidth-broadening techniques, including the multifre-

quency compensation strategy in fixed-beam designs and frequency-dependent compensation schemes in reconfigurable designs, are also applied to further enhance the bandwidth. The reported designs are compared with each other to evoke possible future research directions for the readers.

Acknowledgements

This work was supported in part by the Research Grants Council of the Hong Kong SAR, China (Grant Nos. 9043154 (CityU 11211721) and 9042674 (CityU 11217618)), the National Natural Science Foundation of China (Grant No. 61971370), and the Guangdong Provincial Department of Science and Technology, China (Grant No. 2020B1212030002).

References

[1] D. C. Nguyen, M. Ding, P. N. Pathirana, *et al*., "6G internet of things: A comprehensive survey," *IEEE Internet of Things Journal*, vol. 9, no. 1, pp. 359–383, 2022.

[2] S. Kim, R. Vyas, J. Bito, *et al*., "Ambient RF energy-harvesting technologies for self-sustainable standalone wireless sensor platforms," *Proceedings of the IEEE*, vol. 102, no. 11, pp. 1649–1666, 2014.

[3] J. A. del Peral-Rosado, R. Raulefs, J. A. López-Salcedo, *et al*., "Survey of cellular mobile radio localization methods: From 1G to 5G," *IEEE Communications Surveys & Tutorials*, vol. 20, no. 2, pp. 1124–1148, 2018.

[4] W. Hong, Z. H. Jiang, C. Yu, *et al*., "The role of millimeter-wave technologies in 5G/6G wireless communications," *IEEE Journal of Microwaves*, vol. 1, no. 1, pp. 101–122, 2021.

[5] T. S. Rappaport, Y. C. Xing, O. Kanhere, *et al*., "Wireless communications and applications above 100 GHz: Opportunities and challenges for 6G and beyond," *IEEE Access*, vol. 7, pp. 78729–78757, 2019.

[6] I. F. Akyildiz, C. Han, Z. F. Hu, *et al*., "Terahertz band communication: An old problem revisited and research directions for the next decade," *IEEE Transactions on Communications*, vol. 70, no. 6, pp. 4250–4285, 2022.

[7] A. Mirbeik-Sabzevari, E. Oppelaar, R. Ashinoff, *et al*., "High-contrast, low-cost, 3-D visualization of skin cancer using ultra-high-resolution millimeter-wave imaging," *IEEE Transactions on Medical Imaging*, vol. 38, no. 9, pp. 2188–2197, 2019.

[8] R. Appleby and R. N. Anderton, "Millimeter-wave and submillimeter-wave imaging for security and surveillance," *Proceedings of the IEEE*, vol. 95, no. 8, pp. 1683–1690, 2007.

[9] S. Kurt and B. Tavli, "Path-loss modeling for wireless sensor networks: A review of models and comparative evaluations," *IEEE Antennas and Propagation Magazine*, vol. 59, no. 1, pp. 18–37, 2017.

[10] W. Hong, Z. H. Jiang, C. Yu, *et al*., "Multibeam antenna technologies for 5G wireless communications," *IEEE Transactions on Antennas and Propagation*, vol. 65, no. 12, pp. 6231–6249, 2017.

[11] Y. J. Guo, M. Ansari, R. W. Ziolkowski, *et al*., "Quasi-optical multi-beam antenna technologies for B5G and 6G mmWave and THz networks: A review," *IEEE Open Journal of Antennas and Propagation*, vol. 2, pp. 807–830, 2021.

[12] Y. Li, Z. N. Chen, X. Qing, *et al*., "Axial ratio bandwidth enhancement of 60-GHz substrate integrated waveguide-fed circularly polarized LTCC antenna array," *IEEE Transactions on Antennas and Propagation*, vol. 60, no. 10, pp. 4619–4626, 2012.

[13] J. M. Wen, C. K. Wang, W. Hong, *et al*., "A wideband switched-beam antenna array fed by compact single-layer butler matrix," *IEEE Transactions on Antennas and Propagation*, vol. 69, no. 8, pp. 5130–5135, 2021.

[14] G. H. Sun and H. Wong, "Millimeter-wave high-gain magneto-electric dipole antenna array with pillbox corporate feed network," *IEEE Transactions on Antennas and Propagation*, vol. 69, no. 9, pp. 5631–5639, 2021.

[15] C. Guo, W. Hong, L. Tian, *et al*., "Design and implementation of a full-digital beamforming array with nonreciprocal Tx/Rx beam patterns," *IEEE Antennas and Wireless Propagation Letters*, vol. 19, no. 11, pp. 1978–1982, 2020.

[16] Q. Cheng, L. Zhang, J. Y. Dai, *et al*., "Reconfigurable intelligent surfaces: Simplified-architecture transmitters—From theory to implementations," *Proceedings of the IEEE*, vol. 110, no. 9, pp. 1266–1289, 2022.

[17] H. Yu, J. X. Su, Z. R. Li, *et al*., "A novel wideband and high-efficiency electronically scanning transmitarray using transmission metasurface polarizer," *IEEE Transactions on Antennas and Propagation*, vol. 70, no. 4, pp. 3088–3093, 2022.

[18] G. B. Wu, Y. S. Zeng, K. F. Chan, *et al*., "High-gain filtering reflectarray antenna for millimeter-wave applications," *IEEE Transactions on Antennas and Propagation*, vol. 68, no. 2, pp. 805–812, 2020.

[19] H. Yu, P. Li, J. X. Su, *et al*., "Reconfigurable bidirectional beam-steering aperture with transmitarray, reflectarray, and transmit-reflect-array modes switching," *IEEE Transactions on Antennas and Propagation*, vol. 71, no. 1, pp. 581–595, 2023.

[20] L. Xiao, S. W. Qu, W. Tang, *et al*., "Lightweight, solderless, ultrawideband transmitarray antenna with true-time-delay line," *IEEE Antennas and Wireless Propagation Letters*, vol. 20, no. 12, pp. 2245–2249, 2021.

[21] F. Wu, R. Lu, J. X. Wang, *et al*., "A circularly polarized 1 bit electronically reconfigurable reflectarray based on electromagnetic element rotation," *IEEE Transactions on Antennas and Propagation*, vol. 69, no. 9, pp. 5585–5595, 2021.

[22] Z. L. Wang, Y. H. Ge, J. X. Pu, *et al*., "1 bit electronically reconfigurable folded reflectarray antenna based on p-i-n diodes for wide-angle beam-scanning applications," *IEEE Transactions on Antennas and Propagation*, vol. 68, no. 9, pp. 6806–6810, 2020.

[23] W. X. Yang, K. Chen, S. F. Dong, *et al*., "Full-space dual-helicity decoupled metasurface for a high-efficiency multi-folded reflective antenna," *Optics Express*, vol. 30, no. 19, pp. 33613–33626, 2022.

[24] P. Y. Feng, S. W. Qu, S. W. Yang, *et al*., "Ku-band transmitarrays with improved feed mechanism," *IEEE Transactions on Antennas and Propagation*, vol. 66, no. 6, pp. 2883–2891, 2018.

[25] S. H. R. Tuloti, P. Rezaei, and F. T. Hamedani, "High-efficient wideband transmitarray antenna," *IEEE Antennas and Wireless Propagation Letters*, vol. 17, no. 5, pp. 817–820, 2018.

[26] P. Y. Feng, S. W. Qu, X. H. Chen, *et al*., "Low-profile high-gain and wide-angle beam scanning phased transmitarray antennas," *IEEE Access*, vol. 8, pp. 34276–34285, 2020.

[27] K. M. Luk and H. Wong, "A new wideband unidirectional antenna element," *International Journal of Microwave and Optical Technology*, vol. 1, no. 1, pp. 35–44, 2006.

[28] B. Q. Wu and K. M. Luk, "A broadband dual-polarized magneto-electric dipole antenna with simple feeds," *IEEE Antennas and Wireless Propagation Letters*, vol. 8, pp. 60–63, 2009.

[29] K. Ding, Y. J. Li, and Y. J. Wu, "Broadband circularly polarized magnetoelectric dipole antenna by loading parasitic loop," *IEEE Transactions on Antennas and Propagation*, vol. 70, no. 11, pp. 11085–11090, 2022.

[30] Y. Zhang, X. Y. Zhang, and Q. H. Liu, "Dual-polarized filtering magnetoelectric dipole antenna utilizing intrinsic highpass filter network and integrated lowpass filter network," *IEEE Transactions on Antennas and Propagation*, vol. 69, no. 12, pp. 8090–8099, 2021.

[31] B. T. Feng, J. L. Chen, K. L. Chung, *et al*., "Dual-polarized filtering magneto-electric dipole antenna arrays with high radiation-suppression index for 5G new radio n258 operations," *IEEE Transactions on Antennas and Propagation*, vol. 70, no. 4, pp. 3058–3063, 2022.

[32] Y. J. Li and K. M. Luk, "A 60-GHz wideband circularly polarized

aperture-coupled magneto-electric dipole antenna array," *IEEE Transactions on Antennas and Propagation*, vol. 64, no. 4, pp. 1325–1333, 2016.

[33] X. Dai and K. M. Luk, "A wideband dual-polarized antenna for millimeter-wave applications," *IEEE Transactions on Antennas and Propagation*, vol. 69, no. 4, pp. 2380–2385, 2021.

[34] S. Y. Zhu, Y. L. Li, K. M. Luk, *et al*., "Compact high-gain Si-imprinted THz antenna for ultrahigh speed wireless communications," *IEEE Transactions on Antennas and Propagation*, vol. 68, no. 8, pp. 5945–5954, 2020.

[35] Y. J. Li, C. Wang, and Y. X. Guo, "A Ka-band wideband dual-polarized magnetoelectric dipole antenna array on LTCC," *IEEE Transactions on Antennas and Propagation*, vol. 68, no. 6, pp. 4985–4990, 2020.

[36] J. Sun, A. Li, and K. M. Luk, "A high-gain millimeter-wave magnetoelectric dipole array with packaged microstrip line feed network," *IEEE Antennas and Wireless Propagation Letters*, vol. 19, no. 10, pp. 1669–1673, 2020.

[37] K. M. Luk and B. Q. Wu, "The magnetoelectric dipoleja wideband antenna for base stations in mobile communications," *Proceedings of the IEEE*, vol. 100, no. 7, pp. 2297–2307, 2012.

[38] X. Dai, A. Li, and K. M. Luk, "A wideband compact magnetoelectric dipole antenna Fed by SICL for millimeter wave applications," *IEEE Transactions on Antennas and Propagation*, vol. 69, no. 9, pp. 5278–5285, 2021.

[39] J. Y. Cao, H. Wang, S. X. Mou, *et al*., "W-band high-gain circularly polarized aperture-coupled magneto-electric dipole antenna array with gap waveguide feed network," *IEEE Antennas and Wireless Propagation Letters*, vol. 16, pp. 2155–2158, 2017.

[40] J. R. Reis, M. Vala, and R. F. S. Caldeirinha, "Review paper on transmitarray antennas," *IEEE Access*, vol. 7, pp. 94171–94188, 2019.

[41] S. V. Hum and J. Perruisseau-Carrier, "Reconfigurable reflectarrays and array lenses for dynamic antenna beam control: A review," *IEEE Transactions on Antennas and Propagation*, vol. 62, no. 1, pp. 183–198, 2014.

[42] M. H. Dahri, M. H. Jamaluddin, M. Khalily, *et al*., "Polarization diversity and adaptive beamsteering for 5G reflectarrays: A review," *IEEE Access*, vol. 6, pp. 19451–19464, 2018.

[43] Z. W. Miao, Z. C. Hao, G. Q. Luo, *et al*., "140 GHz high-gain LTCC-integrated transmit-array antenna using a wideband SIW aperture-coupling phase delay structure," *IEEE Transactions on Antennas and Propagation*, vol. 66, no. 1, pp. 182–190, 2018.

[44] F. Wu, J. X. Wang, R. Lu, *et al*., "Wideband and low cross-polarization transmitarray using 1 bit magnetoelectric dipole elements," *IEEE Transactions on Antennas and Propagation*, vol. 69, no. 5, pp. 2605–2614, 2021.

[45] F. Wu, J. X. Wang, L. Xiang, *et al*., "A wideband dual-polarized magneto-electric dipole transmitarray with independent control of polarizations," *IEEE Transactions on Antennas and Propagation*, vol. 70, no. 9, pp. 8632–8636, 2022.

[46] F. Wu, J. X. Wang, R. Lu, *et al*., "A wideband subwavelength-thick circularly polarized discrete lens using dielectric-coated polarization-twisting ME-dipole elements," *IEEE Antennas and Wireless Propagation Letters*, vol. 20, no. 9, pp. 1706–1710, 2021.

[47] F. Wu, L. Xiang, J. X. Wang, *et al*., "A hybrid-element approach to design wideband ME-dipole transmitarray with improved aperture efficiency," *IEEE Antennas and Wireless Propagation Letters*, vol. 21, no. 7, pp. 1338–1342, 2022.

[48] B. Wu, A. Sutinjo, M. E. Potter, *et al*., "On the selection of the number of bits to control a dynamic digital MEMS reflectarray," *IEEE Antennas and Wireless Propagation Letters*, vol. 7, pp. 183–186, 2008.

[49] H. H. Yang, F. Yang, S. H. Xu, *et al*., "A study of phase quantization effects for reconfigurable reflectarray antennas," *IEEE Antennas and Wireless Propagation Letters*, vol. 16, pp. 302–305, 2017.

[50] B. J. Xiang, X. Dai, and K. M. Luk, "A wideband 2-bit transmitarray antenna for millimeter-wave vehicular communication," *IEEE Transactions on Vehicular Technology*, vol. 71, no. 9, pp. 9202–9211, 2022.

[51] F. Diaby, A. Clemente, K. T. Pham, *et al*., "Circularly polarized transmitarray antennas at Ka-band," *IEEE Antennas and Wireless Propagation Letters*, vol. 17, no. 7, pp. 1204–1208, 2018.

[52] J. Huang and R. J. Pogorzelski, "A Ka-band microstrip reflectarray with elements having variable rotation angles," *IEEE Transactions on Antennas and Propagation*, vol. 46, no. 5, pp. 650–656, 1998.

[53] P. Naseri, S. A. Matos, J. R. Costa, *et al*., "Phase-delay versus phase-rotation cells for circular polarization transmit arrays—Application to satellite Ka-band beam steering," *IEEE Transactions on Antennas and Propagation*, vol. 66, no. 3, pp. 1236–1247, 2018.

[54] F. Wu, J. X. Wang, Y. Zhang, *et al*., "A broadband circularly polarized reflectarray with magneto-electric dipole elements," *IEEE Transactions on Antennas and Propagation*, vol. 69, no. 10, pp. 7005–7010, 2021.

[55] X. Dai, G. B. Wu, and K. M. Luk, "A wideband circularly polarized transmitarray antenna for millimeter-wave applications," *IEEE Transactions on Antennas and Propagation*, vol. 71, no. 2, pp. 1889–1894, 2023.

[56] G. B. Wu, S. W. Qu, S. W. Yang, *et al*., "Low-cost 1-D beam-steering reflectarray with ±70° scan coverage," *IEEE Transactions on Antennas and Propagation*, vol. 68, no. 6, pp. 5009–5014, 2020.

[57] J. F. Zhu, Y. Yang, Z. J. Hou, *et al*., "Dual-band aperture-shared high gain antenna for millimeter-wave multi-beam and sub-6 GHz communication applications," *IEEE Transactions on Antennas and Propagation*, vol. 70, no. 6, pp. 4848–4853, 2022.

[58] J. Hu, H. Wong, and L. Ge, "A circularly-polarized multi-beam magneto-electric dipole transmitarray with linearly-polarized feeds for millimeter-wave applications," *IEEE Transactions on Antennas and Propagation*, vol. 70, no. 7, pp. 6012–6017, 2022.

[59] F. Wu, R. Lu, J. X. Wang, *et al*., "Circularly polarized one-bit reconfigurable ME-dipole reflectarray at X-band," *IEEE Antennas and Wireless Propagation Letters*, vol. 21, no. 3, pp. 496–500, 2022.

[60] B. J. Xiang, X. Dai, and K. M. Luk, "A wideband low-cost reconfigurable reflectarray antenna with 1-bit resolution," *IEEE Transactions on Antennas and Propagation*, vol. 70, no. 9, pp. 7439–7447, 2022.

[61] X. Dai, G. B. Wu, and K. M. Luk, "A wideband low-profile reconfigurable transmitarray using magnetoelectric dipole elements," *IEEE Transactions on Antennas and Propagation*, vol. 70, no. 9, pp. 8008–8019, 2022.

[62] T. J. Li, G. M. Wang, H. P. Li, *et al*., "Circularly polarized double-folded transmitarray antenna based on receiver-transmitter metasurface," *IEEE Transactions on Antennas and Propagation*, vol. 70, no. 11, pp. 11161–11166, 2022.

[63] T. J. Li, G. M. Wang, J. G. Liang, *et al*., "A method for transmitarray antenna profile reduction based on ray tracing principle," *IEEE Antennas and Wireless Propagation Letters*, vol. 21, no. 12, pp. 2542–2546, 2022.

[64] M. T. Wang, D. S. Liao, J. Y. Dai, *et al*., "Dual-polarized reconfigurable metasurface for multifunctional control of electromagnetic waves," *IEEE Transactions on Antennas and Propagation*, vol. 70, no. 6, pp. 4539–4548, 2022.

Kwai-Man Luk is a Fellow of the UK Royal Academy of Engineering and a Fellow of the Hong Kong Academy of Engineering Science. He received the B.Sc.(Eng.) and Ph.D. degrees in electrical engineering from The University of Hong Kong in 1981 and 1985, respectively. He joined the Department of Electronic Engineering at City University of Hong Kong in 1985 as a Lecturer. In 1987, he moved to the Department of

Electronic Engineering at The Chinese University of Hong Kong where he spent four years. In 1992, Professor Luk returned to the City University of Hong Kong, where he served as Head of the Department of Electronic Engineering from 2004 – 2010 and Director of State Key Laboratory of Millimeter Waves from 2008 – 2013, and he is currently Acting Head of Department of Electrical Engineering and Chair Professor of Electronic Engineering. His recent research interests include the designs of microstrip patch antennas, magneto-electric dipole antennas, dense dielectric patch antennas and open resonator antennas for wireless connectivity. He is the author of 4 books, 11 research book chapters, over 400 journal papers and 280 conference papers. He was awarded 16 US and more than 10 PRC patents.

Professor Luk received the Japan Microwave Prize, at the Asia Pacific Microwave Conference held in Chiba in December 1994, the Best Paper Award at the International Symposium on Antennas and Propagation held in Taipei in October 2008 and the Best Paper Award at the Asia-Pacific Conference on Antennas and Propagation held in Bali in July 2015. He was awarded the very competitive 2000 Croucher Foundation Senior Research Fellowship in Hong Kong. He received the 2011 State Technological Invention Award (2 Honor) of China. He is the recipient of the 2017 IEEE APS John Kraus Antenna Award for the invention of the L-shaped probe-fed patch antenna and magnetoelectric dipole. He received the prestigious Ho Leung Ho Lee Prize for Science and Technology Progress in 2019 and the 14 Guanghua Engineering Science and Technology Prize in 2022 in China.

He was Lead Guest Editor for the special issue on "Antennas in Wireless Communications" published by the *Proceedings of the IEEE* in July 2012, and for the special issue on "Advanced Antennas for Wireless Connectivity" published by *Engineering*, the flagship journal of the Chinese Academy of Engineering, in April 2022. He is a Deputy Editor-in-Chief of PIERS journals. He served as reviewer of numerous technical journals including *Nature Communications*. Professor Luk is Fellow of the Hong Kong Institution of Engineers, the Chinese Institute of Electronics, the Institution of Engineering and Technology, the Institute of Electrical and Electronics Engineers and the Electromagnetics Academy. (Email: eekmluk@cityu.edu.hk)

Bingjie Xiang received the M.Sc. degree in information and communication engineering from Sun Yat-sen University, Guangzhou, China, in 2018. He is currently working toward the Ph.D. degree in electrical engineering with the City University of Hong Kong, Hong Kong. His current research interests include passive and reconfigurable millimeter-wave antennas and arrays.
(Email: bjxiang2-c@my.cityu.edu.hk)